A Two-Dimensional Model for Melting and Ignition of a Thin Sheared Viscous Layer

R. Timms, R. Purvis
University of East Anglia, Norwich, NR4 7TJ, United Kingdom
R.Timms@uea.ac.uk

ABSTRACT

It is postulated that shear near confining walls is a candidate mechanism for hot spot generation in explosives. However, modelling such an ignition mechanism numerically with hydrocodes proves to offer some considerable challenges. To supplement the numerical approach, we develop an analytical model of the shearing, melting and subsequent ignition of an explosive material. The primary goal of such an approach is to gain a deeper insight into the physical and chemical processes at play. We consider the melting of a thin viscous layer of explosive material due to an applied shear in a idealised planar geometry. A lubrication approximation is made, exploiting the thinness of the melted layer. The mechanics of the problem are solved, enabling the calculation of mechanical dissipation in the melt layer. A single-step Arrhenius reaction is used to model the heating of the explosive due to chemical reactions occurring within the material. The model is used to calculate the temperature increase and temperature localisation in a sample of HMX, allowing potential hot spot locations to be identified.

Introduction

Understanding the mechanisms which have the capability to induce localised temperature increase will aid in the design of safe storage and handling procedures for explosive materials. Mechanical insults resulting from low speed impacts, which shear an explosive, have been identified as a possible ignition source. Investigation of these effects through the use of numerical continuum mechanics methods, such as finite element models, often breaks down owing to problems such as severe mesh deformation (Curtis, 2013). Typically, a very high resolution is required to overcome these issues, but this comes at the cost of computational resources and time. Additionally, large scale numerical codes do not always offer as much physical insight as small scale, simplified, analytical models. Such simplified models are to be employed here to try and gain a deeper understanding of the mechanisms which lead to thermal runaway.

Mechanisms arising from shear are widely discussed in the literature. For instance, Bowden *et al.* (1947), Ubbelohde (1948), Bowden and Gurton (1949), and Bowden and Yoffe (1952) all discuss frictional rubbing as a well established ignition mechanism. During rubbing contact between two solids, the hot spot temperature is determined by the solid with the lower melting point - the lower melting point solid 'quenches' the hot spot temperature to the melting temperature. Bowden and Gurton (1949) were able to measure hot spot ignition temperatures for a wide range of explosives by choosing grits of different melting points and measuring the effect on the sensitivities of the explosives.

Shear localisation has been widely studied in inert materials, see, for example, Bai and Dodd (1992), Dilellio and Olmstead (1997). There have been very few analytical studies on localised shear in explosive materials. However, many experimental studies can be found in the literature. Evidence for localised shear within the explosive sample can be observed in recovered unexploded samples. Photographic evidence for adiabatic shear is given by Field *et al.* (1982), showing ignition and propagation occurring in a shear band in a sample of PETN. Notable work on shear localisation in explosive materials includes: Boyle *et al.* (1989); Chen *et al.* (1997); Dienes (1986); Frey (1980); and the substantial work by Afanas'ev and Bobolev (1971). Also worthy of mention are the experimental works by Howe *et al.* (1986)

and Mohan *et al.* (1989). It is in general concluded that localised shear is a prevalent hot spot mechanism, which manifests in many differing loading scenarios.

Starobin and Dienes (2006) present a one-dimensional model for the lateral melting and ignition of a thin sheared viscous layer. In their work a self similar solution for parabolic melt front propagation in non-reactive materials is found, as well numerical results for non-steady sliding of the crack surface and a non-linear Arrhenius source term. The results presented demonstrate that shear melting in the one-dimensional geometry leads to an increase in the peak hot spot temperature relative to the melting point of HMX.

A natural question arises: will the inhomogeneous structure found in explosive materials cause further localisation? It is to be expected that spatial variations in the explosive material will introduce two-dimensional effects into the propagation of the melt front. In the current work, the one-dimensional model is extended into two spatial dimensions so that the effects of material inhomogeneity can be investigated. In particular, we will assume that a uniform melt layer has already been formed but at some time is perturbed, giving an instantaneous two-dimensional disturbance in the melt front. This will be allowed to evolve in time and its effect on the local temperature field will be studied.

We consider a semi-infinite solid block of explosive material occupying the region $x > 0$, with a rigid wall located at $x = 0$, where x is the horizontal coordinate in the usual Cartesian coordinate system. At time $t = 0$ the wall moves impulsively downwards with speed v_w. The movement provides a shear force on the explosive sample, generating sufficient heat to melt the material near the wall, such that at $t = t_0$ there already exists a thin viscous liquid melt layer adjacent to the wall. The thinness of the melt layer is exploited, and a lubrication analysis is made. Within the lubrication approximation, small deviations from the one-dimensional solution are considered and an asymptotic solution can be found in the case of non-reactive materials. The inclusion of the Arrhenius source term requires solution via a numerical scheme and allows the potential for mechanical hot spots to lead to ignition to be ascertained.

Mathematical Model

Let (u, v) be the velocity components in the (x, y) directions, p be the pressure and T be the temperature. Note, all variables have been non-dimensionalised using typical velocity scale $v^* = v_w$, time scale t^*, density ρ, viscosity μ and temperature difference ΔT. Currently the time scale t^* is chosen to give a correct order of magnitude for the time to thermal runaway when compared with results from experiments. However, further work could be undertaken to calibrate the time scale, thus giving more accurate predictions for the time to runaway.

The melt layer is assumed thin, and in the liquid region we adopt the scalings

$$x = \varepsilon X, \quad u = \varepsilon U, \quad p = \varepsilon^{-2} P, \tag{1}$$

where $\varepsilon = \mathrm{Pe}^{-1/2}$. Here $\mathrm{Pe} = (c_v \rho v_w^2 t^*)/\kappa$ is the Péclet number, which is the ratio of advective transport to diffusive transport, c_v is the specific heat of the explosive material and κ is the thermal conductivity. Under this approximation the governing equations of motion are the lubrication equations

$$\frac{\partial U}{\partial X} + \frac{\partial v}{\partial y} = 0, \tag{2}$$

$$\frac{\partial P}{\partial X} = 0, \tag{3}$$

$$-\frac{\partial P}{\partial y} + \frac{\partial^2 v}{\partial X^2} = 0. \tag{4}$$

The equations [2] – [4] are to be solved subject to no-slip boundary conditions on the wall $X = 0$ and melt front $X = X_f$, that is

$$U = 0, \quad v = -1, \quad \text{on } X = 0, \tag{5}$$

$$U = 0, \quad v = 0, \quad \text{on } X = X_f. \tag{6}$$

We expect that far from the site of the the two dimensional disturbance that the solution will resemble the one dimensional solution, and that the pressure will be constant. It is sufficient to impose the following condition on the pressure

$$\frac{\partial P}{\partial y} \to 0 \quad \text{as } y \to \pm\infty. \qquad [7]$$

The explosive sample is initially heated by viscous dissipation $\Phi = (\partial v/\partial X)^2$ in the melt layer. Once the temperature rise is sufficient, the melt layer is heated further by a consequent chemical reaction. As in Curtis (2013), this is modelled using a single step Arrhenius reaction

$$\frac{\partial \alpha}{\partial t} = \tilde{A}(1-\alpha)\exp\left(-\frac{E}{E(\Delta T)T}\right), \qquad [8]$$

where $\tilde{A} = t^* A$ is the non-dimensional pre-exponential factor, E is the activation energy, R is the molar gas constant and α the mass fraction, ranging from 0 (unreacted) to 1 (fully reacted).

The conservation of energy equation thus reads

$$\frac{\mathrm{D}T}{\mathrm{D}t} = \frac{\partial^2 T}{\partial X^2} + \mathrm{Ec}\,\mathrm{Pr}\,\Phi + \frac{\Omega}{c_v \Delta T}\frac{\partial \alpha}{\partial t}, \qquad [9]$$

where $\mathrm{Ec} = v_w^2/(c_v \Delta T)$ is the Eckert number, $\mathrm{Pr} = (c_v \mu)/\kappa$ is the Prandtl number and Ω is the specific heat of the reaction.

The location of the melt front X_f is determined by the Stefan condition, which equates the temperature flux discontinuity with the magnitude of the latent heat sink at the phase boundary

$$\frac{\partial X_f}{\partial t} = -\mathrm{Ste}\left.\frac{\partial T}{\partial X}\right|_{X=X_f^-}, \qquad [10]$$

where $\mathrm{Ste} = (c_v \Delta T)/L$ is the Stefan number, which is the ratio of sensible heat to latent heat, L. The initial melt front is described in terms of a shape function $S(y)$, that is $X_f(y, t_0) = \tilde{X}_f(t_0) \cdot S(y)$, and is allowed to evolve in time, see Figure 1.

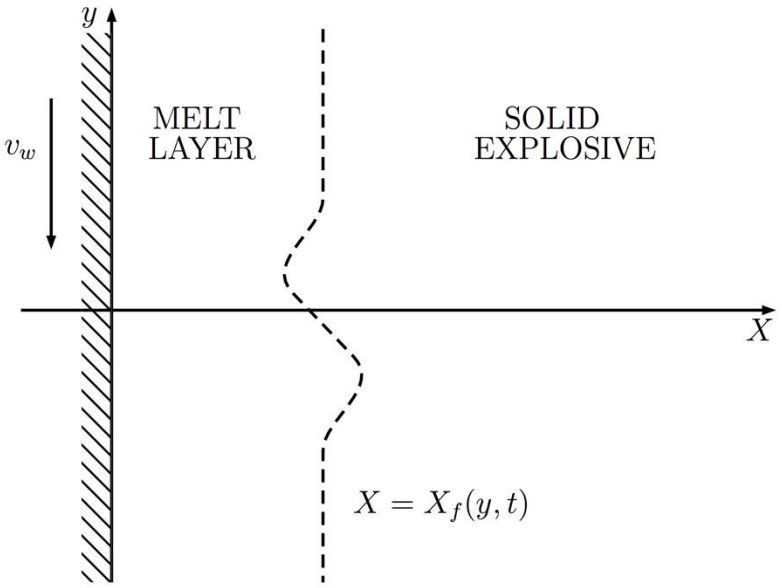

Figure 1: Shear melt layer model.

Equation [4] may be integrated directly to obtain the vertical velocity component v. Application of the no-slip boundary conditions [5] and [6] provides

$$v(X,y,t) = \frac{1}{2}\frac{\partial P}{\partial y}\left(X^2 - X_f X\right) - \left(1 - \frac{X}{X_f}\right). \quad [11]$$

The pressure gradient may be calculated in terms of the melt front shape X_f by integration of the mass continuity equation [2] across the melt layer

$$\frac{\partial P}{\partial y} = -\frac{6}{X_f^3}\int_{-\infty}^{y} \frac{\partial X_f}{\partial y'}\,\mathrm{d}y'. \quad [12]$$

The horizontal velocity component may be calculated from the continuity equation [2] as

$$U(X,y,t) = 2\frac{\partial X_f}{\partial y}\frac{X^2}{X_f^2}\left(1 - \frac{X}{X_f}\right), \quad [13]$$

where the pressure gradient terms have been eliminated through use of equation [12].

The temperature $T(X,y,t)$ may be determined numerically by solution of the energy equation [9]. Note that all mechanical aspects may now be calculated analytically from the velocity components [11] and [13]. For small times it can be shown that equation [9] reduces to a simplified, one-dimensional form, and a self-similar solution is available. This solution provides an initial condition for the numerical computations.

Results

Results are given for a sample of HMX subject to a uniform wall speed v_w. See Table 1 for material properties of HMX. It is assumed that at time $t = t_0$ a melt layer has already been formed, and two-dimensional effects are introduced via the imposed shape function $S(y)$. Such effects may manifest physically as a result of the inhomogeneous nature of the explosive material. For example, material properties may locally differ in space, causing some areas to melt more rapidly than others, thus resulting in a non-uniform melt width. The aim of this work is not to describe how such two-dimensionality may arise, but to study the effects spatial variations in the melt front may have on the temperature field and time to runaway.

Table 1: Material properties for HMX, taken from Starobin and Dienes (2006) and Curtis (2013).

Explosive Property	**HMX**
Activation Energy E	2.2×10^5 J mol^{-1}
Heat of Reaction Ω	5.02×10^6 J Kg^{-1}
Molar Gas Constant R	8.314 J kg^{-1}K^{-1}
Pre-Exponential Constant A	$5.011872336 \times 10^{19}$s^{-1}
Density ρ	1860 kg m^{-3}
Viscosity μ	4.6×10^{-2}kg m^{-1}s^{-1}
Latent Heat L	2.08×10^5J kg^{-1}
Melting Temperature T_m	520.6 K
Specific Heat c_v	989.25 J kg^{-1}K^{-1}
Thermal Conductivity κ	0.404 W m^{-1}K^{-1}

A number of melt front shapes were studied. Here we draw comparison between two shapes, parametrised by δ: $S_1(\delta, y) = 1 + (\delta/2)e^{-y^2}$ and $S_2(\delta, y) = 1 + \delta e^{-y^2}\sin(\pi y)$. For shape S_1 negative values of δ correspond to a perturbation towards the wall, whilst positive values of δ correspond to perturbations away from the wall. Shape S_2 has perturbations towards and away from the wall, and captures both heating mechanisms present in shape S_1 for positive and negative δ. These shapes were selected to allow investigation of disturbances away from and towards the wall both in isolation and in conjunction with one another.

Somewhat counterintuitively, we find that widening the initial melt layer, as in S_1 with $\delta > 0$, appears to be the most violent initial condition in the sense of decreasing time to runaway. It is found that the heating due to mechanical dissipation is greatest adjacent to the wall and opposite from the imposed disturbance in the melt front, see Figure 2(a). The temperature rise here is sufficient to kickstart a local reaction, causing the temperature to rise rapidly. This has the resultant effect of causing the disturbance to grow in magnitude, causing further temperature localisation. Thus the overall time to runaway is reduced when compared with the one-dimensional case. The high contribution of heating due to reaction is clearly depicted in Figure 2.

The evolution of the melt front, along with the temperature profiles across the width of the melt layer, is shown in Figure 3(a). Although not clear here, the perturbation to the melt front initially decays, but then grows again once the reaction kicks in. That is, we may say the chemical reaction serves to destabilise perturbations from a uniform melt layer. This can be seen more clearly in Figure 3(b) which depicts the perturbation from the uniform melt layer at a series of increasing times. We see that towards the end of the computation the disturbance begins to grow again, albeit only by a small amount by the time the ignition threshold was reached. Looking at the temperature across the melt width, we observe a temperature rise of over 200K near the reaction site. However, away from the reaction site we see that the temperature profile across the melt width has remained almost unchanged throughout the duration of the computation.

In shapes which cause a narrowing of the melt layer (i.e. S_1 with $\delta < 0$) we find the dissipation to be greatest at the melt front, see Figure 4(a). The additional temperature increase near the unmelted explosive material causes the melt front to propagate more quickly, so does not have the effect of decreasing the time to runaway. We find that the hot spot generated by the narrowing of the melt layer is quenched to the melt temperature T_m by the solid explosive and that the melt front flattens. We conclude that a hot spot located on the melt front has little or no effect on the time to runaway. Indeed, we observe that the chemical reaction finally takes off on the wall, but away from the site of the localised disturbance, see Figure 4(b). This is further illustrated in Figure 5, where we observe that the temperature increase is less near the disturbance, see Figure 5(c), than it is away from the disturbance, see Figure 5(d). In this case the reaction takes longer to kick off, and we observe a noticeable temperature increase throughout the melt layer over the duration of the computation. We again observe that the disturbance initially decays and then grows subsequent to the initiation of chemical reaction, see Figure 5(b). In this case, since the reaction occurs on the wall away from the perturbation, the bulk of the melt layer propagates ahead of the narrow area, resulting in the apparent growth of the perturbation in the later stages of melting.

When both widening and narrowing effects are present, as in S_2, both mechanical heating mechanisms are present, see Figure 6(a). We observe an increase in dissipation on the wall opposite the widening part of the disturbance, and an increase in the dissipation on the melt front adjacent to the narrowing part of the disturbance. Whilst the heating due to dissipation is increased in two locations, only one of these mechanical hot spots is sufficient to trigger a chemical reaction. Figure 6(b), shows the heating due to chemical reaction at 568 ns for a sample of HMX with initial melt front shape S_2. It is clear to observe that the heating on the wall has led to a significant reaction, whereas the heating on the melt front has not. This is again evident in the temperature field, where we see a temperature increase of over 50K at the reaction site compared with the maximum temperature in the far field, Figure 6(c). Recall that the mechanical hot spot on the melt front is quenched to the melting temperature T_m. For this particular computation, runaway occurred at time 631 ns. At the time of reaction, the peak temperature is c. 300 K higher than the maximum temperature in the far field.

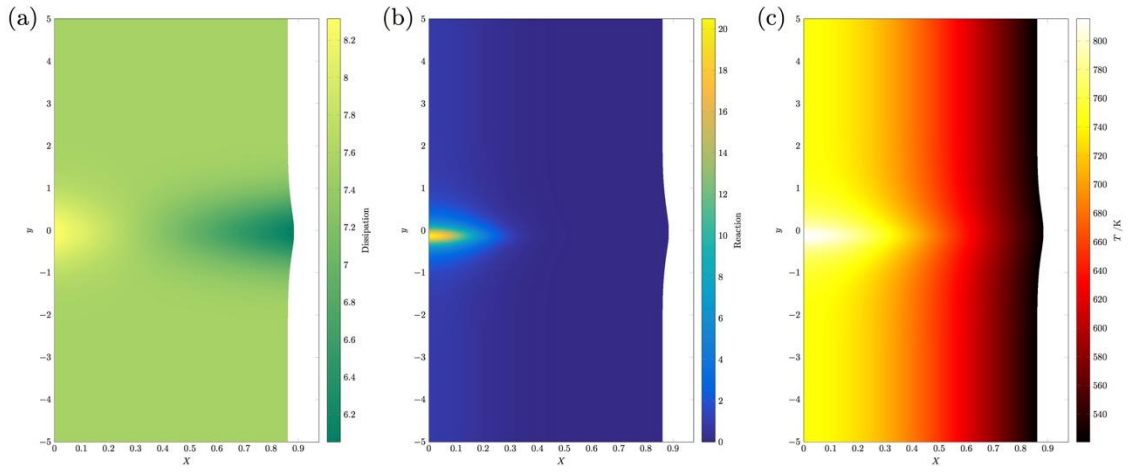

Figure 2: (a) Non-dimensional instantaneous energy increase due to mechanical dissipation; (b) Non-dimensional instantaneous energy increase due to reaction; and (c) Dimensional temperature (K) of a sample of HMX at 90% of the time to runaway since t_0. An initial melt front shape $S_1(0.8, y)$ and wall speed $v_w = 70$ m s^{-1} were used. [Original in colour.]

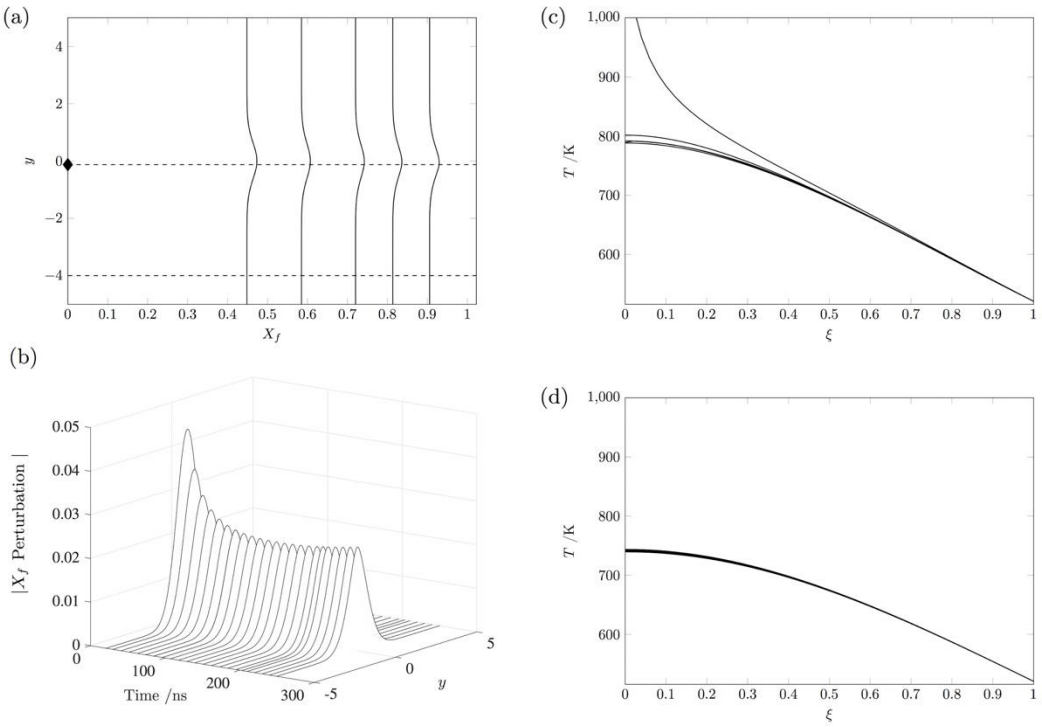

Figure 3: (a) Melt front location at times $t = 59, 108, 158, 207, 256$ ns for a sample of HMX with initial melt front shape $S_1(0.8, y)$; and (b) the magnitude of the melt front perturbation at a series of increasing times. Also shown are temperature profiles across the melt width at the times depicted in (a), plotted at vertical coordinates: (c) $y = y_R$ where y_R is the vertical coordinate of the peak reaction site, and (d) $y = -4$. The filled diamond symbol shows the location of the peak reaction site at ignition. The dashed lines in (a) show the locations of the temperature profiles taken in (c) and (d). A wall speed $v_w = 70$ m s^{-1} was used.

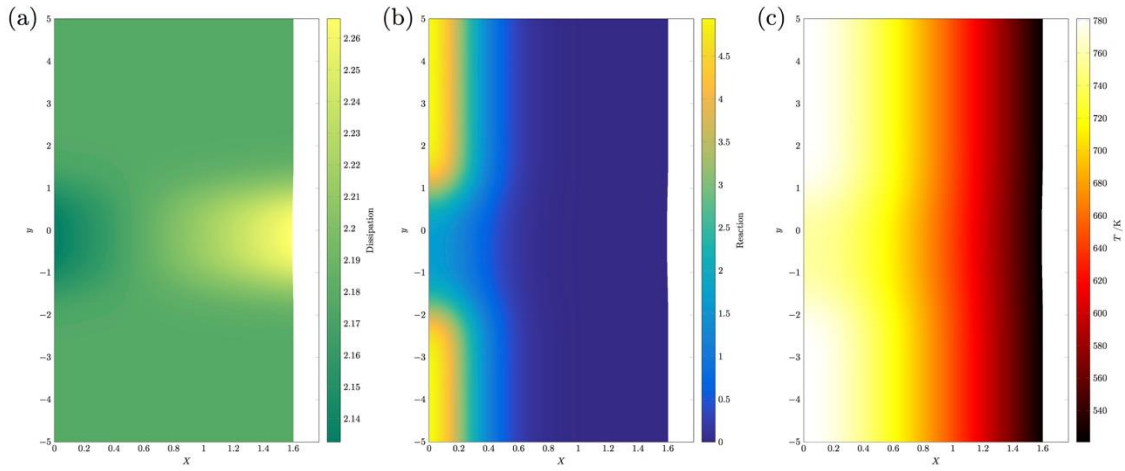

Figure 4: (a) Non-dimensional instantaneous energy increase due to mechanical dissipation; (b) Non-dimensional instantaneous energy increase due to reaction; and (c) Dimensional temperature (K) of a sample of HMX at 90% of the time to runaway since t_0. An initial melt front shape $S_1(-0.8, y)$ and wall speed $v_w = 70\ \mathrm{m\ s^{-1}}$ were used. [Original in colour.]

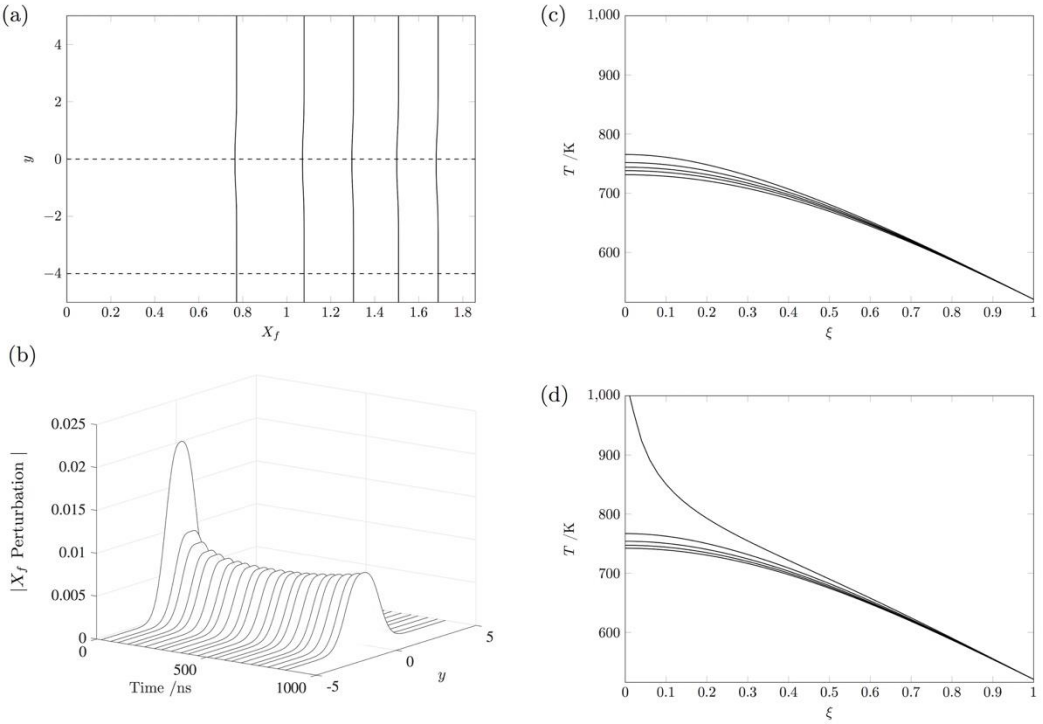

Figure 5: (a) Melt front location at times $t = 186, 357, 530, 704, 877$ ns for a sample of HMX with initial melt front shape $S_1(-0.8, y)$; and (b) the magnitude of the melt front perturbation at a series of increasing times. Also shown are temperature profiles across the melt width at the times depicted in (a), plotted at vertical coordinates: (c) $y = 0$, and (d) $y = -4$. The dashed lines in (a) show the locations of the temperature profiles taken in (c) and (d). A wall speed $v_w = 70\ \mathrm{m\ s^{-1}}$ was used.

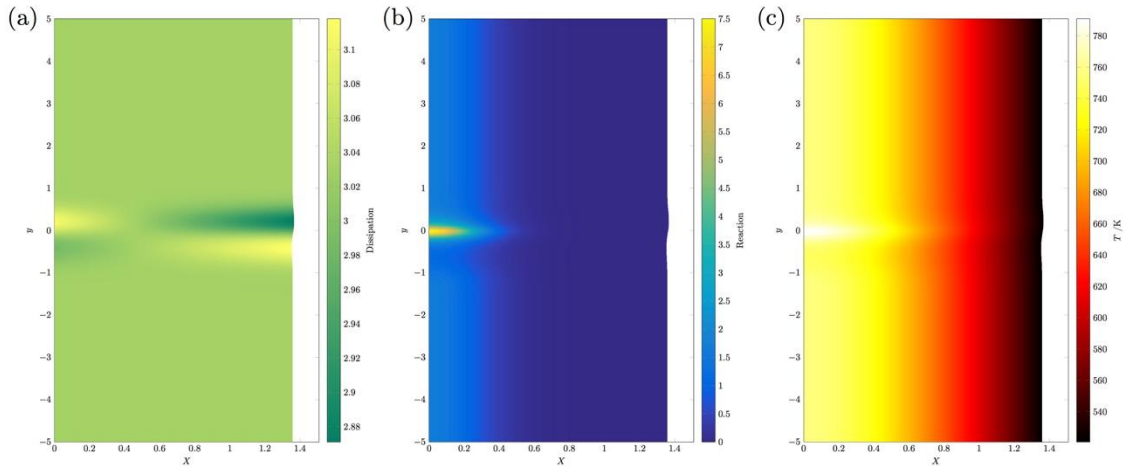

Figure 6: (a) Non-dimensional instantaneous energy increase due to mechanical dissipation; (b) Non-dimensional instantaneous energy increase due to reaction; and (c) Dimensional temperature (K) of a sample of HMX at 90% of the time to runaway since t_0. An initial melt front shape $S_2(0.5, y)$ and wall speed $v_w = 70\ \mathrm{m\ s^{-1}}$ were used. [Original in colour.]

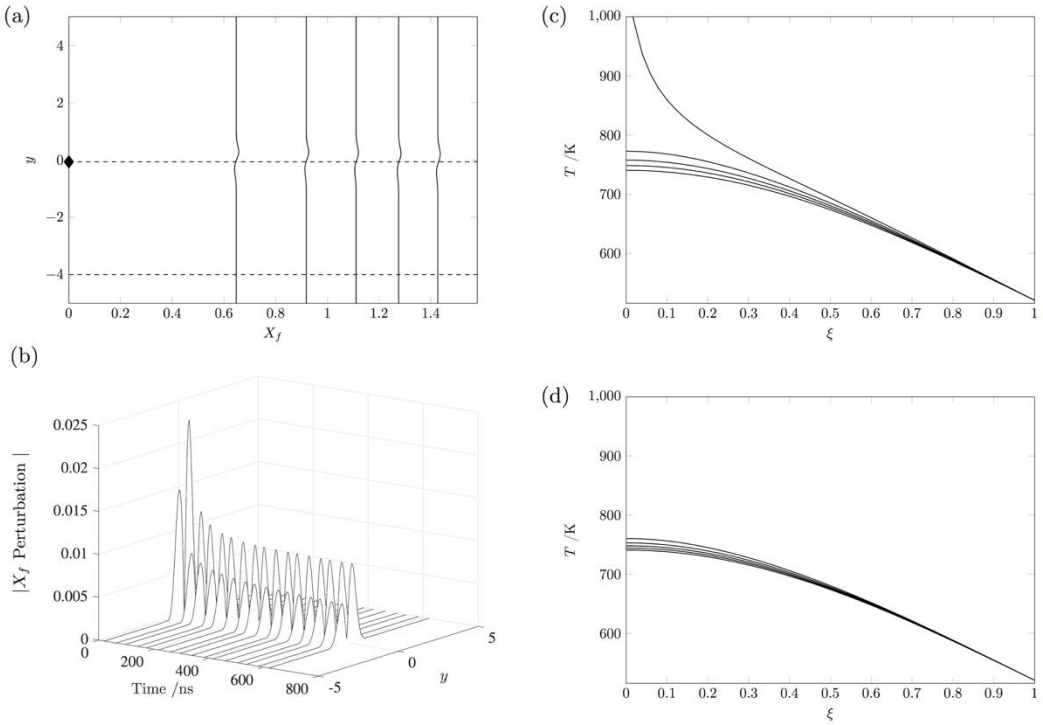

Figure 7: (a) Melt front location at times $t = 134, 258, 383, 507, 631$ ns for a sample of HMX with initial melt front shape $S_2(0.5, y)$; and (b) the magnitude of the melt front perturbation at a series of increasing times. Also shown are temperature profiles across the melt width at the times depicted in (a), plotted at vertical coordinates: (c) $y = y_R$ where y_R is the vertical coordinate of the peak reaction site, and (d) $y = -4$. The filled diamond symbol shows the location of the peak reaction site at ignition. The dashed lines in (a) show the locations of the temperature profiles taken in (c) and (d). A wall speed $v_w = 70\ \mathrm{m\ s^{-1}}$ was used.

If we consider the evolution of the melt front for imposed shape S_2, we observe that the narrowing effect of the melt front perturbation has diminished, whereas the widening effect remains throughout the computation, see Figure 7. Note that the initial perturbation had components of equal magnitude towards and away from the wall. We may draw contrast between these differing effects. The hot spot caused by the narrowing perturbation, which is located on the melt front, causes the melting of further solid material, thus flattening the melt front profile. However, the hot spot caused by the perturbation away from the wall kick starts a reaction, which exacerbates the perturbation, and the melt front is perturbed further from the wall. We may conclude that perturbations away from the wall persist, whereas perturbations towards the wall quickly decay. This is demonstrated numerically, where we always observe a reduced time to ignition when a perturbation away from the wall is included.

The time to ignition as a function of δ for both shapes $S_1(\delta, y)$ and $S_2(\delta, y)$ is shown in Figure 8. The quenching behaviour is clearly demonstrated – for perturbations which only serve to narrow the melt width, we see that the ignition time is unchanged from that of a uniform melt layer. This is due to the fact that hot spots generated on the melt front are not sufficient to kick start a chemical reaction. When hot spots occur both on the wall and on the melt front, i.e. as in shape S_2, we see that the ignition time decreases as $|\delta|$ increases. In this case changing δ changes the location of the hot spot, but there is always a hot spot located on the moving wall which is sufficient to start a chemical reaction.

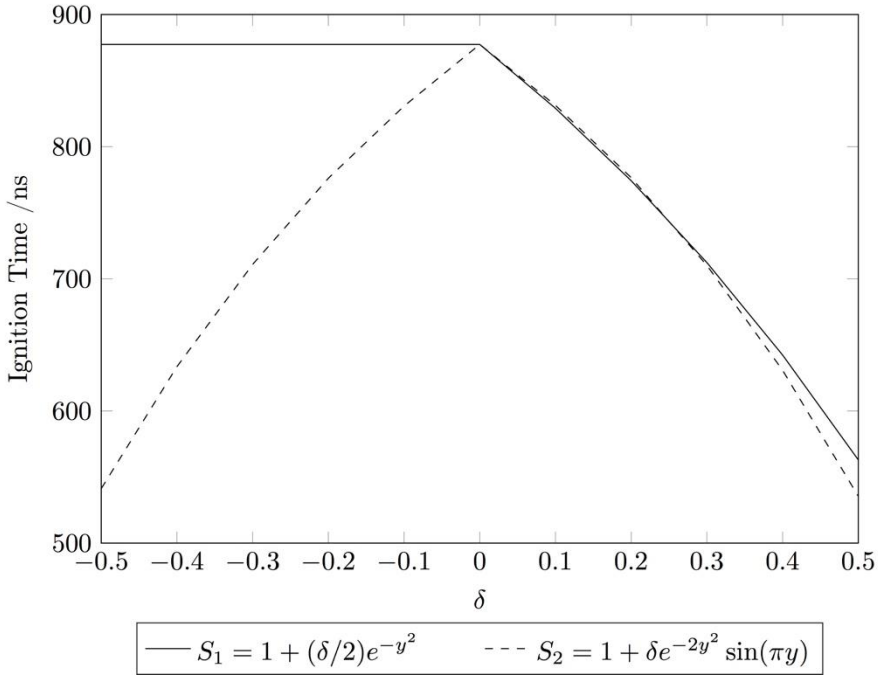

Figure 8: Time to ignition as a function of δ for initial melt front shapes S_1 and S_2.

Conclusions

The numerical results presented here indicate that variations from a uniform width melt layer can indeed cause localised heating due to mechanical dissipation. This leads to so called hot spots in the melted explosive material. Interestingly, it appears that whilst different geometries all give rise to temperature localisation, they can have substantially different effects on the time to runaway, dependent on the hot spot location. It is clear from the results that the geometry of the melt layer is crucial in determining the outcome of temperature localisation and, ultimately, time to runaway. Whilst the results highlight the mechanisms available for hot spot generation, the predicted times to runaway are advisory. Further work is needed to validate the numerical results and calibrate model parameters in order to fit some experimental test cases.

In order to investigate any two-dimensional effects, highly idealised melt front shapes were selected. A more realistic scenario may, for example, involve choosing a shape which coincides with the grain size of the explosive material in question or with typical dimensions of grit found within the explosive. Although the grain size may be significantly larger than some of the melt thicknesses studied so far, such an approach may be more appropriate for slower wall speeds where the melt layer thickness is allowed to increase further before ignition. Polymer bonded explosives are highly granular materials, and the constituent materials in the explosive will in general have different thermomechanical properties. Such spatial differences in material properties will inevitably create a non-uniform melt layer. Alternatively, it may be of interest to consider a scenario where the melt front encounters a small air gap in the explosive material.

For this study many material properties, such as specific heat and viscosity, were assumed constant with respect to pressure and temperature. Whilst this may be a reasonable simplification it is worth noting that the predicted ignition times would need to be reconsidered in order to account for the effects which are not included, such as thermal softening. Future work may include a more detailed study of the effects of varying material properties, allowing for dependence on temperature, stress etc. Additionally, it is worth noting that the wall has been treated as perfectly insulated, whereas in reality there may be some heat loss to the confining wall.

An alternative interpretation of the current work would be to consider a scenario in which an internal crack develops, and two material planes slide against one another. In this case the rigid wall may be replaced with a symmetry condition at $X = 0$, as in Starobin and Dienes (2006). In any case, the heating mechanisms discussed here would still be present.

Acknowledgements

Thanks to EPSRC for financial support via an industrial CASE partnership with AWE [grant number EP/L505729/1]. Thanks are also due to John Curtis and colleagues at AWE for useful scientific discussions.

References

(1) Curtis, J.P.; *Explosive ignition due to adiabatic shear.* Proceedings of the 39th International Pyrotechnics Seminar, Denver, Colorado, 2013.
(2) Bowden, F.P.; Mulcahy, M.F.R; Vines, R.G.; Yoffe, A. The detonation of liquid explosives by gentle impact. The effect of minute gas spaces. *Proc. R. Soc. Lond.* **1947**, A 188, 291-311.
(3) Ubbelohe, A.R. Part iii. (4) Mechanical and thermal processes of initiation. *Phil. Trans. of the R. Soc. Lond.* **1948**, A 241, 280-286.
(4) Bowden, F.P.; Gurton, O.A. Initiation of solid explosives by impact and friction: The influence of grit. *Proc. R. Soc. Lond.* **1949**, A 198, 337-349.
(5) Bowden, F.P.; Yoffe, A.D. *Initiation and growth of explosions in liquids and solids.* Cambridge University Press, 1952.
(6) Bai, Y.L.; Dodd, B. *Adiabatic shear localization: Occurrence, theories and applications.* Pergamon Press, Oxford, 1992.
(7) Dilellio, J.A.; Olmstead, W.E. Shear band formation due to a thermal flux inhomogeneity. *SIAM Journal on Applied Mathematics* **1997**, 57, 959-971.
(8) Field, J.E.; Swallowe, G.M.; Heavens, S.N. Ignition mechanisms of explosives during mechanical deformation. *Proc. R. Soc. Lond.* **1982**, A 382, 231-244.
(9) Boyle, V.; Frey, R.; Blake, O. *Combined pressure shear ignition of explosives.* Proceedings of the 9th Symposium (International) on Detonation, 1989.
(10) Chen, H.C.; Nesterenko, V.F.; LaSalvia, J.C.; Meyers, M.A. Shear-induced exothermic chemical reactions. *Le Journal de Physique* **1997**, IV 7.
(11) Dienes, J.K. On reactive shear bands. *Physics Letters* **1986**, A 118, 433-438.
(12) Frey, R.B. *The initiation of explosive charges by rapid shear*. Technical Report, DTIC Document, 1980.
(13) Afanas'ev, G.T.; Bobolev, V.K. *Initiation of solid explosives by impact.* Isreal Program for Scientific Translations, 1971.
(14) Howe, P.M.; Gibbons Jr, G.; Webber, P.E. *An experimental investigation of the role of shear in initiation of detonation by impact.* Technical Report, DTIC Document, 1986.
(15) Krishna Mohan, V.; Jyothi Bhasu, V.C.; Field, J.E. *Role of adiabatic shear bands in initiation of explosives by drop-weight impact.* Proceedings of the 9th Symposium (International) on Detonation, 1989.
(16) Starobin, A.J.; Dienes, J.K. One-dimensional thermomechanical model for lateral melting and ignition of a thin sheared viscous layer. *Combustion Theory and Modelling* **2006**, 10, 885-905.